Importance of solvent roles in molecular, electronic and dynamical properties, thermodynamic quantities, Mulliken charges, reactive analysis and molecular docking of 2-Bromo-1H-imi...

Article *in* Journal of Molecular Liquids · August 2023

DOI: 10.1016/j.molliq.2023.122744

CITATION
1

READS
109

4 authors, including:

Rajesh Pv
School of Basic Sciences, Vels Institute of Science Technology & Advanced Studies…
39 PUBLICATIONS **122** CITATIONS
SEE PROFILE

Sambanthan Muthu
Govt Thirumagal Milss College,Gudiyattum,Vellore Dist,Tamilnadu,India
315 PUBLICATIONS **5,662** CITATIONS
SEE PROFILE

Journal of Molecular Liquids 388 (2023) 122744

Contents lists available at ScienceDirect

Journal of Molecular Liquids

journal homepage: www.elsevier.com/locate/molliq

Importance of solvent roles in molecular, electronic and dynamical properties, thermodynamic quantities, Mulliken charges, reactive analysis and molecular docking of 2-Bromo-1H-imidazole-4,5-dicarbonitrile

M. Lawrence [a,b,*], P. Rajesh [a], Ahmad Irfan [c], S. Muthu [d]

[a] Department of Physics, Vels Institute of Science, Technology and Advanced Studies (VISTAS), Chennai, Tamil Nadu 600117, India
[b] Department of Physics, Loyola Institute of Technology, Chennai, Tamil Nadu 600123, India
[c] Department of Chemistry, College of Science, King Khalid University, Abha 61413, P.O. Box 9004, Saudi Arabia
[d] Department of Physics, Arignar Anna Govt. Arts College, Cheyyar 604 407, Tamil Nadu, India

ARTICLE INFO

Keywords:
DFT
AIM
Solvation
NLO
MEP
Molecular docking

ABSTRACT

The 2-Bromo-1H-imidazole-4,5-dicarbonitrile (2B1HID) molecule is studied by quantum mechanical and vibrational spectroscopic methods. Atoms In Molecules (AIM) was carried out to find the topological studies and know the type of bonding present in it. The calculations of NBO studies are used to determine the solidity. By HOMO and LUMO analysis various chemical parameters and band gaps were determined. The TD-DFT approach is used with the help of simulated UV–Vis with various solvents to know the electronic transition. Explanation of the Fukui function and studies of Molecular Electrostatic Potential demonstrate the molecule's bioactive nature and reactive areas. NLO studies were carried out to find Non-linear applications of the molecule. Thermodynamic studies confirm that this molecule's important parameters increase with an increase in temperature. By using drug-likeness, the drug characters of the molecule are obtained. By molecular docking, the target protein and the ligand reactions were examined.

1. Introduction

Life cannot exist without a functional kidney. The kidney is the complex organ that regulates blood pressure, red blood cell count, fluid volume bone density, and acts as a key homeostasis regulator. Nephron production occurs throughout the fetal stage in humans, as in most mammals, with the ultimate nephron count being determined prior to or shortly after birth. The discovery that human nephron numbers vary by a factor of ten between individuals, that newborns are unable to develop new nephrons, and that there is a distinct inverse link between nephron quantity and renal illness has brought the development of the kidney back into the spotlight [1–4]. For blood filtration, solute and water excretion/absorption, and body fluid equilibrium, the vertebrate kidney is essential for the elimination of metabolic waste. The nephron is the main component of the kidney and it is physically and functionally conserved throughout vertebrates. It is made up of two main components: the renal tubules and the glomerular. The glomerulus produces ultrafiltrate, which travels into the tubules where it is successively changed by selective solute reabsorption and secretion [5–6]. Based on the prediction of the organic compounds biological activity using the PASS online, this titled compound is used to treat renal failure treatment [7–9].

A careful review of the literature reveals that vibrational spectroscopic studies, docking experiments, and there have been no quantum analyses for evaluating the chemical's precise target. This encourages research into comprehensive DFT in the compound's vibrational spectroscopic and the electronic transition was studied by UV–Vis using different solvents. Natural bond orbital analysis (NBO) is a technique that may be used to find the stability of 2B1HID. The topological characteristics and electron energy density are obtained by applying the concept of atoms in molecules (AIM). Using bandgap it is possible to determine a molecule's reactivity and stability. Utilising the concept of molecular electrostatic potential (MEP), the reactive area and molecule shape are determined. NLO and thermodynamic studies have also been carried out on this compound. The ADME drug-likeness studies confirm the drug characters of the title compound. Finally, the molecular docking experiments show how the heading molecule interacts with many proteins in an appropriate way, which explains its potential for

* Corresponding author at: Department of Physics, Vels Institute of Science, Technology and Advanced Studies (VISTAS), Chennai, Tamil Nadu 600117, India.
E-mail address: mawrence2051971@gmail.com (M. Lawrence).

https://doi.org/10.1016/j.molliq.2023.122744
Received 26 May 2023; Received in revised form 25 July 2023; Accepted 2 August 2023
Available online 3 August 2023

renal disease treatment and antifungal properties.

1.1. Computational method

The DFT technique is used to compute the structure of 2B1HID using the Gaussian 09 application with the aid of B3LYP / 6–311++G (d, p) approach [10] and GaussView 06 [11] was used to derive the geometric parameters and other molecular features. AIM calculations are carried out using a multiwfn program [12]. All calculations were performed using DFT and TD-DFT concepts. Using AutoDock Suite 4.2.1 [13] the ligand–protein interactions were calculated. Using PyMol [14] and VMD [15] programs the visible representations are generated.

2. Results and discussions

2.1. Optimization of the structure

The stable and optimized structure of 2B1HID is displayed in Fig. 1. The investigational values were obtained from a similar structure [16]. The XRD indicates that the structure is monoclinic, P21/n, with intercepts of 7.3217 Å (6), 12.8128 Å (11), and 7.5202 Å (6) and symmetry Z = 4. Table 1 displays the bond analysis of 2B1H1D. The obtained bond length for C-N results are within the theoretical range of 1.305 to 1.156 Å. The length of the N–H bond is roughly 1.010 Å due to the intense interaction between the nitrogen and hydrogen atoms. The C–C bonds have a longer bond length of 1.420 Å.

2.2. Vibrational analysis

From Table 2., 2B1HID has 27 vibrational modes. Based on the vibrations, unscaled values were obtained. For the basis set B3LYP a small scaling factor of 0.96 is used. The Raman and IR values are tabulated along different functional groups along with corresponding PED values. The calculated IR and Raman spectra are shown in Fig. 2 and Fig. 3.

2.3. N–H vibration

3400 to 3700 cm^{-1} is the range for N–H stretching vibrations [17,18]. Here unscaled values are observed at 3629 cm^{-1} and the reduced factor values are at 3487 cm^{-1}. The IR intensity is 67 and the Raman activity is 12.

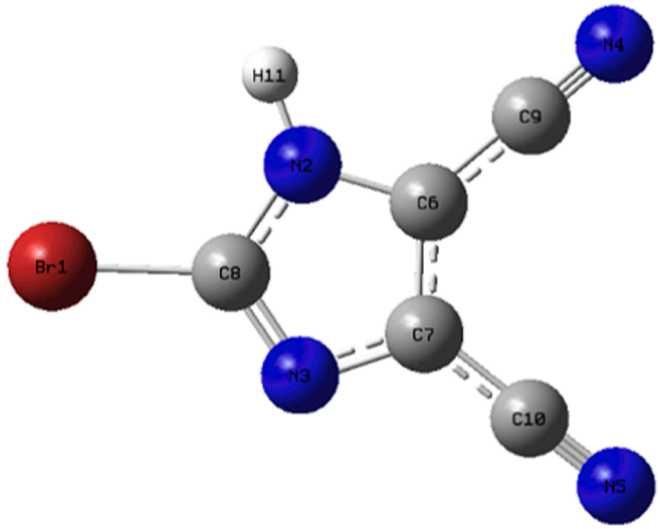

Fig. 1. Optimized geometric structure with atom numbering of 2B1HID.

Table 1
Geometrical parameters optimized in 5ADCPP, bond length (Å) and bond angle (°).

Bond length (Å)		Bond angle (°)	
Br1-C8	1.873	Br1-C8-N2	121.5
N2-C6	1.382	Br1-C8-N3	125.8
N2-C8	1.362	C6-N2-C8	106.8
N2-H11	1.010	C6-N2-H11	126.3
N3-C7	1.374	N2-C6-C7	104.7
N3-C8	1.305	N2-C6-C9	123.1
N4-C9	1.156	C8-N2-H11	126.9
N5-C10	1.154	N2-C8-N3	112.7
C6-C7	1.388	C7-N3-C8	105.2
C6-C9	1.410	N3-C7-C6	110.5
C7-C10	1.420	N3-C7-C10	122.5
		N4-C9-C6	179.2
		N5-C10-C7	179.3
		C7-C6-C9	132.2
		C6-C7-C10	127.0

2.4. C–C vibrations

The mixed mode vibrations including stretching vibrations of C–C was located at 1571, 1371, and 1180 cm^{-1}, and the scaled frequencies are observed at 1510, 1317, and 1134 cm^{-1}[19,20].

2.5. C–N–H vibrations

The C–H–N vibrations are observed at 1571, 1485, 1419, and 1180 cm^{-1} and the related scaled values are 1510, 1427, 1363, and 1134 cm^{-1} [21]. These vibrations exist with the mixed vibrations along with the stretching vibrations of NC. The PED contributions are 13%, 15 %, 15%, and 44% respectively and these values are quite low due to the presence of mixed mode vibrations.

2.6. C-N vibrations

1335 to 1250 cm^{-1} and 1650 to 1550 cm^{-1} is the range for C-N vibrations. The bands observed at 1485, 1419, 1371, and 1281 cm^{-1} and their related scaled values are 1427, 1363, 1317, and 1231 cm^{-1}. The PED contributions are 36%, 61%, 58%, and 71% respectively.

2.7. AIM study

The bonding between two atoms is calculated based bond's critical point. The quantum theory is utilized to study the type of energy and bonds [22,23]. Fig. 4 displays the molecular structure of the AIM. The AIM parameters are tabulated in Table 3. The bond is covalent when $\nabla^2 \rho_{BCP}$ and $H_{BCP} < 0$. It is said to be partially covalent if $\nabla^2\rho_{BCP} > 0$ as well as $H_{BCP} < 0$. If $\nabla^2 \rho_{BCP} > 0$ and $H_{BCP} > 0$, then it represents the weak bond.

The interaction energy of the hydrogen bond is obtained by

$$E_{H\ldots X} = ½(1/4\ \nabla^2\rho - 2\ Gc)$$

From Table 3, Br1-C8 has higher internal energy compared to other bonds.

2.8. Non-covalent interactions – DORI analysis

The covalent and noncovalent interactions are studied using a single function called density overlap regions indicator (DORI) [24,25]. It was discovered that, with the right isovalue selection, the DORI isosurface may display both covalent and noncovalent interaction zones, and sign (2) can also be mapped onto DORI isosurfaces to simplify interaction nature analysis. DORI depict the covalent and non-covalent interactions. From Fig. 5, there are two noncovalent interactions available between N4 and N5 and another one at the centre of the cycle. Fig. 6 describes the

Table 2
Simulated vibrational frequency with assignments for FODHCC.

No	Calculated DFT/B3LYP/6–311 + G(d,p)				Assignments (PED)[a]
	Unscaled cm^{-1}	scaled[b] cm^{-1}	IR intensity[c]	Raman activity	
1	3629	3487	67	12	γNH(1 0 0)
2	2352	2260	7	62	γNC(85) + γCC(12)
3	2336	2245	20	100	γNC(85) + γCC(12)
4	1571	1510	14	20	βCNC(37) + βHNC(13) + βNCN(15) + γCC(22)
5	1485	1427	84	13	γNC(36) + βHNC(15) + βNCN(12)
6	1419	1363	7	8	γNC(61) + βHNC(15) + βCNC(20)
7	1371	1317	62	14	γNC(58) + γCC(24)
8	1281	1231	23	6	γNC(71) + βCNC(10)
9	1180	1134	2	1	γNC(14) + γCC(24) + βHNC(44)
10	1143	1099	17	0	γNC(42) + βCNC(15)
11	990	951	9	2	γNC(23) + βNCN(45) + βCNC(22)
12	712	685	0	1	τCNCN(56) + OUTCCNC(23)
13	701	673	1	1	γBrC(11) + γCC(68) + βNCN(11)
14	680	653	2	0	τHNCN(20) + τCNCN (48) + OUTBrNNC(15)
15	662	636	2	0	βNCC(29) + βCCC(27) + βCCN(21)
16	552	531	47	0	τHNCN(76) + τCNCN (14)
17	533	512	1	1	τNCCN(37) + τNCCC (29) + OUTCNCC(15) + OUTCCNC(11)
18	528	507	0	0	γCC(37) + βCNC(49)
19	489	470	1	1	βNCC(53) + βCCC(14) + βCCN(10)
20	461	443	0	0	τNCCN(32) + τNCCC (33) + τCNCN(25)
21	319	307	1	1	γBrC(68)
22	293	282	3	0	βBrCN(47) + βNCC(40)
23	254	244	3	0	τNCCC(11) + OUTBrNNC(44) + OUTCCNC(12) + OUTCNCC(15)
24	154	148	3	0	τNCCN(10) + τNCCC (13) + OUTCCNC(32) + OUTCNCC(31)
25	134	129	2	0	βNCC(27) + βCCC(12) + βCCN(19) + βBrCN (35)
26	107	103	2	2	βNCC(36) + βCCC(33) + βCCN(25)
27	101	97	3	0	OUTBrNNC(33) + OUTCCNC(21) + OUTCNCC(23)

d Relative Raman intensities normalized to 100.
[a] υ - stretching, β - bending, τ – torsion, vw – very weak, w – weak, m – medium, s – strong, vs – very strong.
[b] scaling factor: 0.961 for B3LYP/6–311++G(d,p).
[c] Relative absorption intensities normalized with highest peak absorption equal to 100.

contour map of the title compound. Around the Br1 atom, more concentric circles imply the negative region. Similarly, more concentric circles are available around all the carbon atoms. It describes the size and shape of the molecule in 2D representation.

2.9. NBO

By using second-order perturbation theory, the donor and acceptor orbital along with the inter and intramolecular reactions for all the electronic structures can be determined using the given equation [26–28].

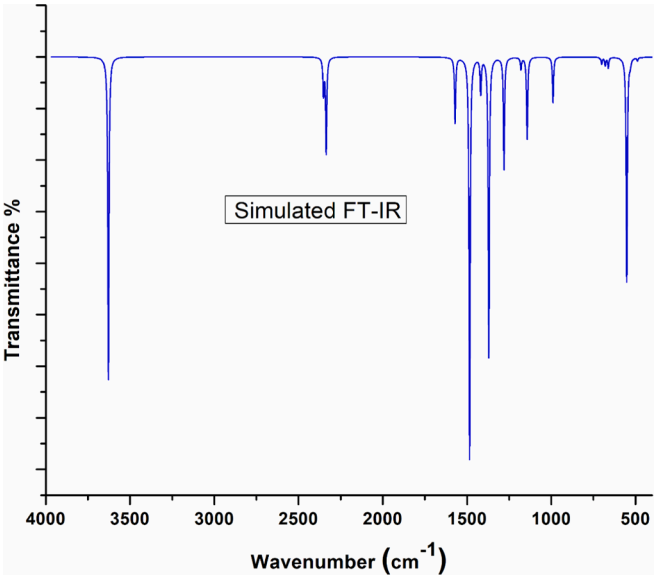

Fig. 2. Simulated FT-IR spectrum.

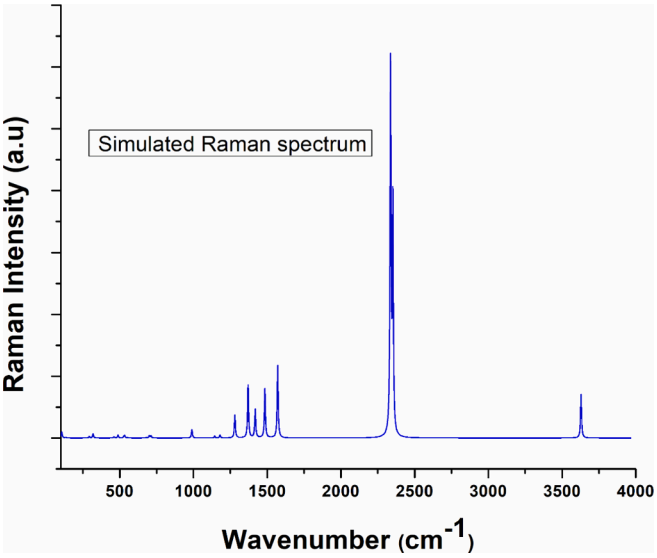

Fig. 3. Simulated FT-Raman spectrum.

$$E_2 = \Delta E_{ij} = q_i \frac{F(i,j)^2}{E_i - E_j}$$

E_2 – stabilization energy
q_i – Orbital (donor) occupancy
Ei and Ej – orbital energies
F(i,j) – Fock and Kohn-Sham elements of matrix.

The important interactions are listed in Table 4. The range of π(N3-C8) to π*(C6-C7) has the maximum stabilization energy, with a value of 65.47 kcal/mol. With an energy value of E2 48.01 kcal/mol, from LP1 (N2) lone pair electrons of N2 is donated to π*(N3-C8). The donor's LP1 (N2), π (C6-C7), and π(N3-C8) transfer energy to orbital of acceptors π* (C6-C7), π* (N4-C9), and π* (C6-C7) with stabilization energies of 35.32 kcal/mol, 25.83 kcal/mol, and 20.99 kcal/mol are important transitions for the stability of 2B1HID.

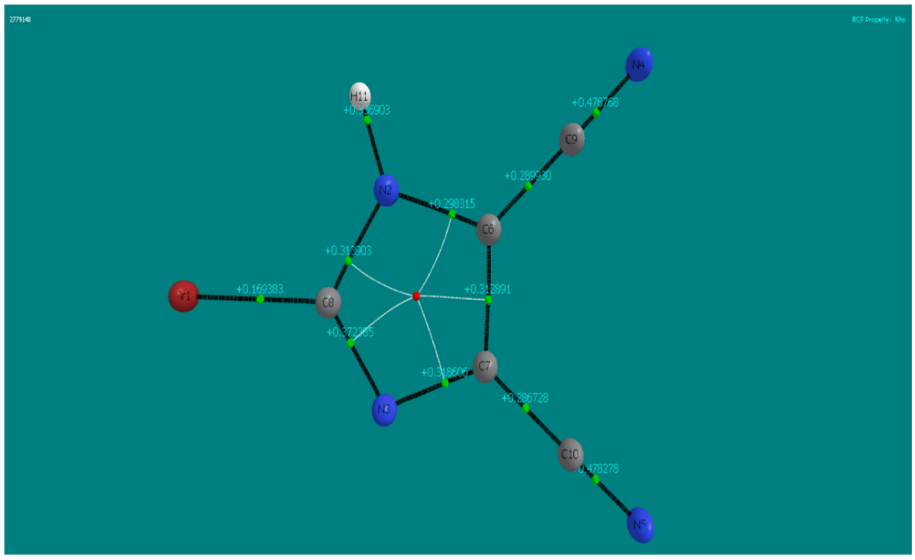

Fig. 4. AIM molecular diagram of 2B1HID.

Table 3
Bonding, density, ellipticity, Internal energy of 5ADCPP by AIM theory.

BCP	Atoms	ρBCP	∇^2 ρ DelSqRho	Ellipticity	G	V	H	MOD(V)/G	D. E(int) kcal/mol
1	N2 - C8	0.3139	−0.7836	0.2541	0.2448	−0.6855	−0.4407	2.8003	−0.7294
2	N3 - C8	0.3724	−1.1255	0.2851	0.2658	−0.8129	−0.5471	3.0587	−0.6151
3	N2 - C6	0.2983	−0.7131	0.2344	0.2296	−0.6375	−0.4079	2.7765	−0.7843
4	N3 - C7	0.3186	−0.9130	0.1657	0.1760	−0.5803	−0.4043	3.2966	−0.8616
5	C6 - C7	0.3129	−0.8500	0.3501	0.1114	−0.4353	−0.3239	3.9070	−1.1485
6	C6 - C9	0.2899	−0.8082	0.1146	0.0837	−0.3695	−0.2858	4.4136	−1.3533
7	N4 - C9	0.4768	−0.2621	0.0262	0.7934	−1.6523	−0.8589	2.0826	−0.3026
8	C7 - C10	0.2867	−0.8053	0.1011	0.0785	−0.3583	−0.2798	4.5648	−1.3954
9	N5 - C10	0.4783	−0.2461	0.0247	0.8015	−1.6645	−0.8630	2.0768	−0.3004
10	Br1 - C8	0.1694	−0.1517	0.0826	0.0645	−0.1668	−0.1024	2.5883	−2.9970
11	N2 - *H*11	0.3369	−1.7556	0.0403	0.0449	−0.5288	−0.4838	11.7658	−0.9456

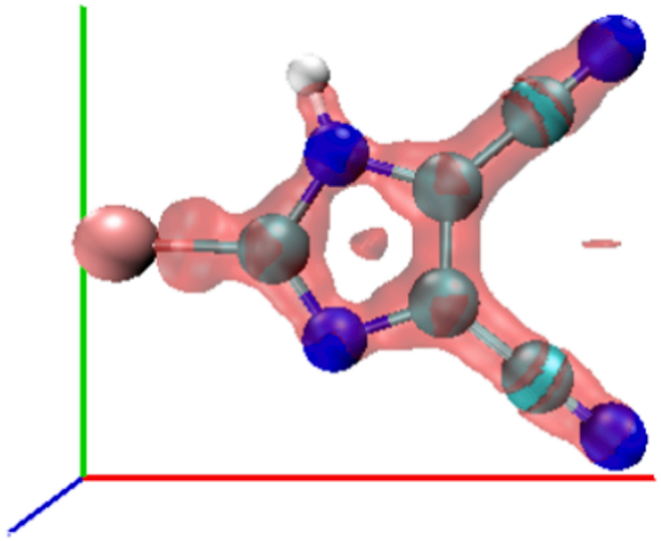

Fig. 5. DORI analysis of 2B1HID.

2.10. *Frontier molecular orbital*

It is crucial to find the bioactive nature, and electrical as well as optical characteristics using the frontier molecular orbital analysis [29,30]. The HOMO and LUMO values are used to determine the chemical potential, chemical hardness, and chemical softness and are tabulated in Table 5. This molecule appears to be relatively stable and bioactive based on its band gap value of 5.1008 eV as shown in Fig. 7. The ionization potential is 7.8459 eV and it is comparatively very low. The term "electron affinity" and its numerical value of 2.7451 refer to the energy changes that occur when an atom gains an electron. The chemical potential is −5.2955 eV and it suggests high stability. Thus, the compound 2B1HID can be implied to be biologically active.

2.11. *Effect of solvents – UV–Vis study*

UV light is employed in a variety of biological studies and investigations. The solvents such as ethanol, methanol, and DMSO were used for simulating the UV–Visible spectra using the TD-DFT method [31,32]. A new correlation function with hybrid exchange named CAM-B3LYP procedure is followed [33,34]. With 2B1HID, the UV absorption spectrum varies depending on the concentration of each and every solvent. Depending on the solvent's polarity, a pi-pi transition or an n-pi transition takes place. Table 6 displays each solvent's maximum absorption wavelength, energy, frequency (F), and assignments, including ethanol, methanol, DMSO, and gas. The primary transition for 2B1H1D occurs at 243.98 nm, 244.80 nm, 244.21 nm, and 237.88 nm for methanol, DMSO, ethanol, and at the gas phase. The majority of HOMO to LUMO contribution (94%) is observed with the addition of methanol as the solvent. Fig. 8 displays the UV–Vis spectra of 2B1H1D's in the gas phase and with the solvents; each spectrum obtained for the solvents contains two dominating peaks.

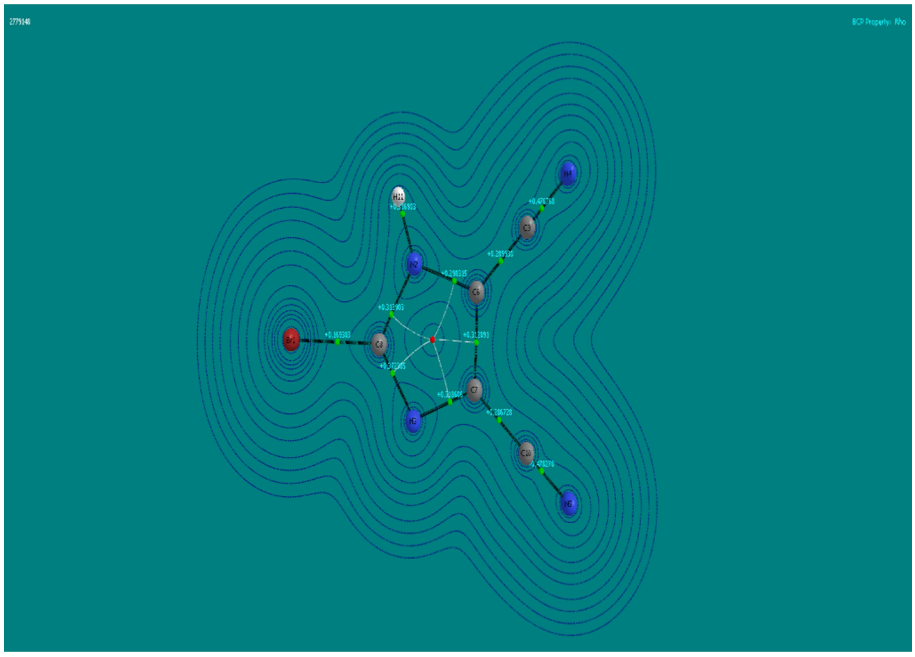

Fig. 6. Contour diagram of 2B1HID.

Table 4
Second order perturbation theory analysis of Fock matrix in NBO basis for 5ADCPP.

DonorNBO(i)	Type	ED/e	AcceptorNBO(j)	Type	ED/e	E(2) kcal/mol	E(j)-E(i) a.u.	F(i,j) a.u.
N2-C6	σ	1.974	Br1-C8	σ*	0.044	5.22	0.92	0.062
N3-C7	σ	1.959	Br1-C8	σ*	0.044	8.90	0.86	0.078
N3-C8	π	1.839	C6-C7	π*	0.402	20.99	0.34	0.080
N4-C9	σ	1.994	C6-C9	σ*	0.030	6.95	1.52	0.092
N4-C9	π	1.977	N2-C6	σ*	0.028	5.76	0.77	0.059
N5-C10	σ	1.994	C7-C10	σ*	0.034	6.90	1.52	0.092
C6-C7	σ	1.966	C6-C9	σ*	0.030	5.01	1.24	0.071
C6-C7	π	1.772	N3-C8	π*	0.398	14.60	0.27	0.059
C6-C7	π	1.772	N4-C9	π*	0.090	16.76	0.39	0.075
C6-C7	π	1.772	N5-C10	π*	0.070	14.19	0.41	0.071
C6-C9	σ	1.981	N4-C9	σ*	0.009	6.96	1.64	0.096
C7-C10	σ	1.982	N5-C10	σ*	0.009	7.09	1.64	0.097
Br1	LP(2)	1.960	N2-C8	σ*	0.051	6.03	0.71	0.059
Br1	LP(3)	1.923	N3-C8	π*	0.398	14.06	0.28	0.061
N2	LP(1)	1.567	N3-C8	π*	0.398	48.01	0.27	0.103
N2	LP(1)	1.567	C6-C7	π*	0.402	35.32	0.30	0.093
N3	LP(1)	1.913	N2-C8	σ*	0.051	8.12	0.79	0.072
N3	LP(1)	1.913	C6-C7	σ*	0.037	5.50	0.94	0.065
N4	LP(1)	1.974	C6-C9	σ*	0.030	11.43	1.02	0.097
N5	LP(1)	1.974	C7-C10	σ*	0.034	11.29	1.02	0.096
N3-C8	π	0.398	C6-C7	π*	0.402	65.47	0.03	0.063
C6-C7	π	0.402	N4-C9	π*	0.090	25.83	0.09	0.088
C6-C7	π	0.402	N5-C10	π*	0.070	20.67	0.11	0.088

‘

Table 5
Calculated energy values of 5ADCPP.

Parameters	Values eV
HOMO(eV)	−7.8459
LUMO(eV)	−2.7451
Ionization potential	7.8459
Electron affinity	2.7451
Energy gap(eV)	5.1008
Electronegativity	5.2955
Chemical potential	−5.2955
Chemical hardness	2.5504
Chemical softness	0.1960
Electrophilicity index	5.4976

2.12. Molecular electrostatic potentials (MEP)

MEP is useful for analyzing the structural function of the compound [35–37]. It gives significant and practical information about the binding process, charge transfer, and reactive areas vulnerable to electrophilic and nucleophilic assaults. Fig. 9 displays the reactive zones of the 2B1H1D present. The various reactive areas are represented by different coloured surfaces. Electrophilic reactivity is constituted by red, and nucleophilic reactivity is constituted by blue. As the negative potential areas have been found around the nitro group, the MEP investigation of the molecule indicated promising places around the NC group.

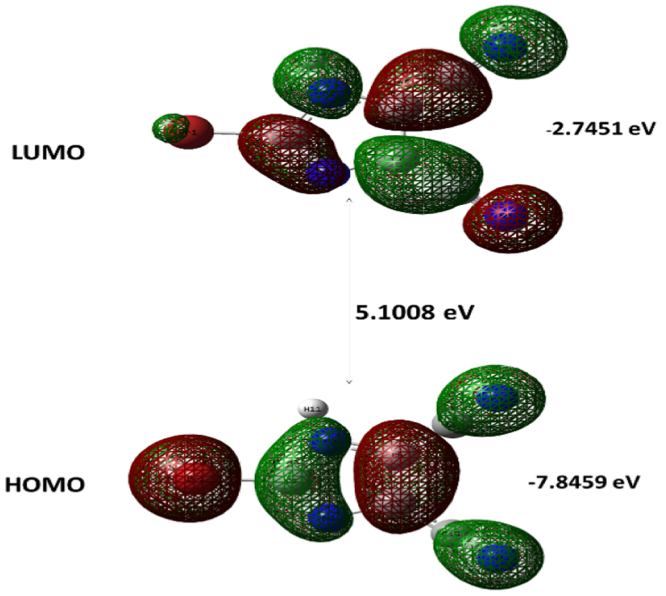

Fig. 7. Frontier molecular orbital of 2B1HID.

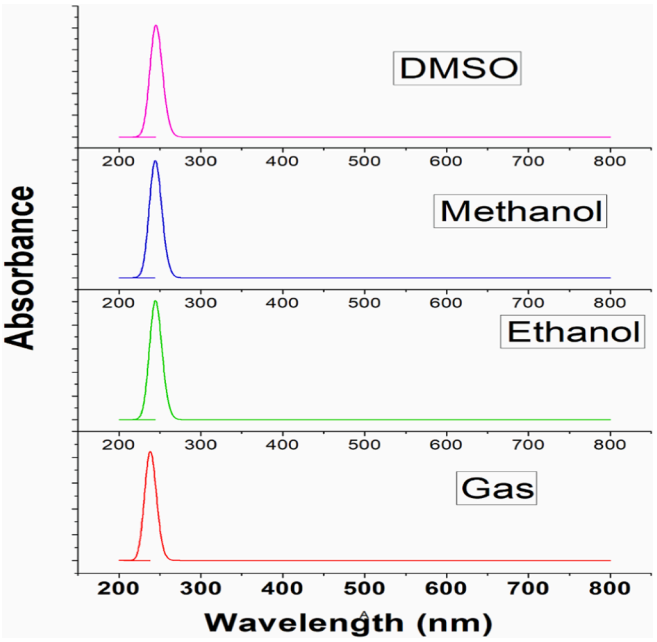

Fig. 8. Simulated UV spectrum of 2B1HID with various solvents.

Table 6
The UV–vis absorption wavelength (λ_{max}) and oscillator strength (f) for 5ADCPP.

Solvent	Energy (cm-1)	Wavelength (nm)	Osc. Strength (f)	Major contribs
Methanol	40,987	243.98	0.3426	HOMO->LUMO (94%)
	44,734	223.54	0.0005	HOMO->L + 1 (85%)
	49,363	202.58	0.0001	H-3->LUMO (12%), HOMO->L + 2 (−16%), HOMO->L + 4 (45%)
dmso	40,850	244.80	0.3538	HOMO->LUMO (94%)
	44,729	223.57	0.0005	HOMO->L + 1 (85%)
	49,367	202.56	0.0001	H-3->LUMO (11%), HOMO->L + 2 (−15%), HOMO->L + 4 (45%)
Ethanol	40,949	244.21	0.3472	HOMO->LUMO (94%)
	44,726	223.58	0.0005	HOMO->L + 1 (85%)
	49,353	202.62	0.0001	H-3->LUMO (12%), HOMO->L + 2 (−16%), HOMO->L + 4 (44%)
gas	42,038	237.88	0.2916	HOMO->LUMO (94%)
	44,062	226.95	0.0002	HOMO->L + 1 (82%)
	48,465	206.33	0.0002	HOMO->L + 2 (41%), HOMO->L + 4 (28%)

2.13. Fukui function

The quantitative values of charges of each and individual atom for the entire molecule is represented by the Fukui function which is based on Mulliken charges [38,39]. The Fukui function is calculated by,

$$f(\vec{r}) = \left(\frac{\partial \rho}{\partial N}\right) v(\vec{r}) = \left(\frac{\delta \mu}{\delta v(\vec{r})}\right) N$$

The core calculation of the Fukui technique is employed atomic marking to identify the parts of the molecular region that are zonally reactive. The dual descriptor of each atom of the Fukui function is shown in Table 7. Due to the lower dual descriptor, C6 may be a target for an electrophilic assault. The reactivity sequence for the electrophilic

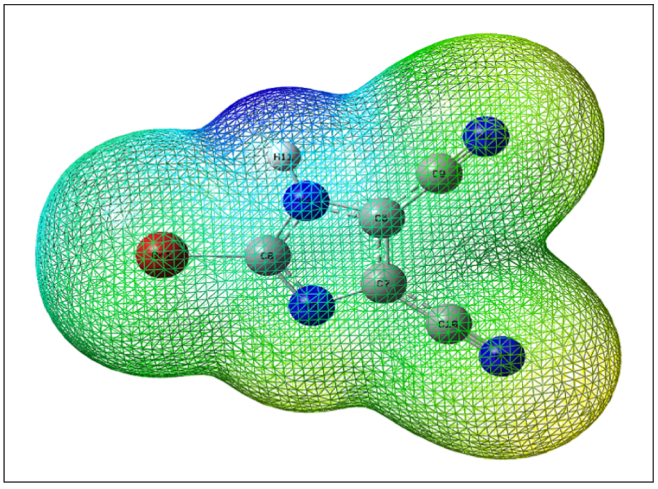

Fig. 9. Molecular Electrostatic Potential (MEP) of 2B1HID.

condition is predicted by the table using MPA [40,41] schemes and it is in the order of C6 > C7 > N4 > N5 > C8. The nucleophilic attack is in the order of C9 > Br1 > N3 > C10 > N2 > *H*11. In comparison with nucleophilic and radical attacks, 2B1HID has a stronger electrophilic attack. These results show that the 2B1HID molecule has a stronger biological activity.

2.14. Non-linear optical effects

Non-linear optical features are shown by organic materials used in many optical effects [42,43]. The DFT approach is used to calculate the 2B1HID 's NLO activity. The prototype molecule called urea is used to check the NLO properties of the heading compound. As urea is widely applied as a significant drug for comparison purposes. The obtained NLO values for 2B1HID are shown in Table 8. The β value of 2B1HID is 3.1380×10^{-30} esu and the total μ is 2.6179 D. It exemplifies 2B1HID has potent NLO characteristics.

Table 7
Condensed Fukui function *f*r and new descriptor (*sf*)r for 5ADCPP.

Atom	Mulliken atomic charges			Fukui functions			local softness			Dual descriptor
	N (0,1)	N + 1 (−1, 2)	N-1 (1,2)	fr +	fr -	fr 0	sr+ *f*r+	sr-*f*r-	sr0 *f*r0	
Br1	0.0271	−0.1456	0.2986	−0.1727	−0.2715	−0.2221	−0.0361	−0.0568	−0.0464	0.0988
N2	−0.1121	−0.1570	−0.0594	−0.0449	−0.0527	−0.0488	−0.0094	−0.0110	−0.0102	0.0078
N3	−0.0110	−0.0677	0.0815	−0.0567	−0.0925	−0.0746	−0.0119	−0.0193	−0.0156	0.0358
N4	−0.1492	−0.3548	0.0224	−0.2056	−0.1717	−0.1886	−0.0430	−0.0359	−0.0394	−0.0339
N5	−0.1552	−0.3339	0.0095	−0.1786	−0.1647	−0.1717	−0.0374	−0.0344	−0.0359	−0.0139
C6	1.3629	1.1727	1.3973	−0.1902	−0.0344	−0.1123	−0.0398	−0.0072	−0.0235	−0.1558
C7	1.6344	1.4770	1.6929	−0.1574	−0.0585	−0.1079	−0.0329	−0.0122	−0.0226	−0.0989
C8	0.2268	0.2187	0.2298	−0.0080	−0.0030	−0.0055	−0.0017	−0.0006	−0.0012	−0.0050
C9	−1.7428	−1.6928	−1.6585	0.0500	−0.0844	−0.0172	0.0105	−0.0176	−0.0036	0.1344
C10	−1.4397	−1.4252	−1.4246	0.0145	−0.0151	−0.0003	0.0030	−0.0032	−0.0001	0.0296
*H*11	0.3589	0.3085	0.4105	−0.0504	−0.0516	−0.0510	−0.0105	−0.0108	−0.0107	0.0012

Table 8
The calculated dipole moment μ (D), polarizability (α_0), first-order hyperpolarizability (βtot) components of 5ADCPP.

Parameters	Values	Parameters	Values
μ_x	−2.1503	β_{xxx}	125.6076
μ_y	1.4931	β_{xxy}	−30.5286
μ_z	−0.0003	β_{xyy}	−65.4068
μ(D)	**2.6179**	β_{yyy}	109.7976
α_{xx}	148.8877	β_{zxx}	−0.9623
α_{xy}	1.4660	β_{xyz}	0.7237
α_{yy}	108.3838	β_{zyy}	−0.4260
α_{xz}	−0.0021	β_{xzz}	−2.4912
α_{yz}	−0.0020	β_{yzz}	3.7415
α_{zz}	52.1359	β_{zzz}	0.1487
α_a(e.s.u)	**1.5285E-23**		
Δα (e.s.u)	**4.0202E-23**	βtot (e.s.u)	**3.1380E-30**

2.15. Effect of temperature

The average body temperature of an adult ranges by 20 °C. The temperature variance of the 2B1HID thermodynamic characteristics was determined using the Perl script. Table 9 provides the computed values of the thermodynamic variables. The values of temperature are taken from 100 K to 1000 K. At 100 K the values are 289.70 J/Mol.k, 67.63 J/Mol.k, and 4.74 KJ/Mol respectively. The values for the thermodynamic parameters increase to 610.87 J/Mol.k, 219.50 J/Mol.k, and 156.39 KJ/Mol when the temperature is elevated to 1000 K. As illustrated in Fig. 10, the entropy, heat capacity, and enthalpy show a raise as the temperature raises. This demonstrates the high thermal stability of 2B1HID [44,45].

2.16. Drug likeness

The software SwissADME [46] computes the crucial drug parameters based on the input mol file which contains the basic atomic structure and composition. The crucial drug-like characteristics based on Lipinski's rule are tabulated in Table 10 [47,48]. The HBA, HBD, RB, MR, and TPSA are the important parameters for Drug-Likeness. The chart demonstrates that for all of the aforementioned characteristics of the compound and there are no Lipinsky violations in it. The bioavailability score for compound 2B1HID is 0.55. We deduce that the 2B1HID is appropriate to be used as the drug for renal disease from the aforementioned parameter.

Table 9
Variation of thermodynamic properties with temperature.

T (K)	S (J/mol.K)	Cp (J/mol.k)	ddH (kJ/mol)
100	289.70	67.63	4.74
200	347.85	103.57	13.33
298.15	394.80	132.32	24.97
300	395.62	132.79	25.22
400	437.06	155.45	39.67
500	473.73	173.14	56.14
600	506.57	187.00	74.18
700	536.25	197.94	93.44
800	563.28	206.67	113.69
900	588.04	213.73	134.72
1000	610.87	219.50	156.39

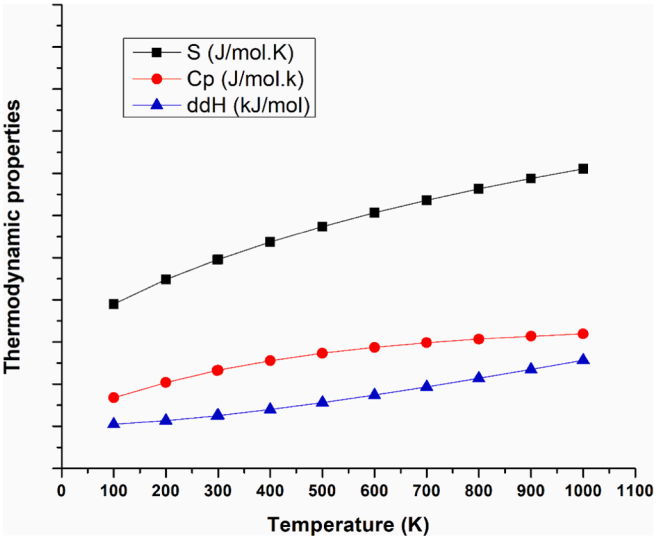

Fig. 10. Variation of thermodynamic properties with temperature.

2.17. Molecular docking

The appropriate target protein for 2B1HID is chosen from the literature review and online way2drug software [49] utilized for renal disease medications. The docking parameters are displayed in Table 11. The protein ID 4ZRT is acquired from the protein data bank website, and the Ramachandran plot is used to assess the protein's quality and whether the protein is not damaged [50]. This is a crucial protein present in the Nephrin and is for the proper functioning of renal filtration [51]. Fig. 11 demonstrates that 4ZRT is a good-quality protein as its amino acids are present in designated areas. According to the literature review in the introduction section, the title compound is effective for renal disease. The obtained binding energy for the 4ZRT with 2B1HID is −6.36 kcal/mol [52–55]. For 2B1HID the docking diagram is displayed in Fig. 12. This demonstrates the efficacy of 2B1HID as a compound for renal disease treatment.

Table 10
ADME Characters of 5ADCPP.

Molecule	H-bond acceptors	H-bond donors	MR	TPSA	Lipinski violations	Bioavailability Score
2-Bromo-1H-imidazole-4,5-dicarbonitrile	3	1	35.72	76.26	0	0.55

Table 11
Molecular docking with ligand and 4ZRT target protein.

Protein (PDB ID)	Bonded residues	No. of hydrogen bond	Bond distance (Å)	Estimated Inhibition Constant (μm)	Binding energy (kcal/mol)	Reference RMSD (Å)
4ZRT	GLN266 GLY220 ILE219 GLY218	5	1.9 1.8 2.1	21.73	−6.36	15.341
SER215 2.1		2.7				

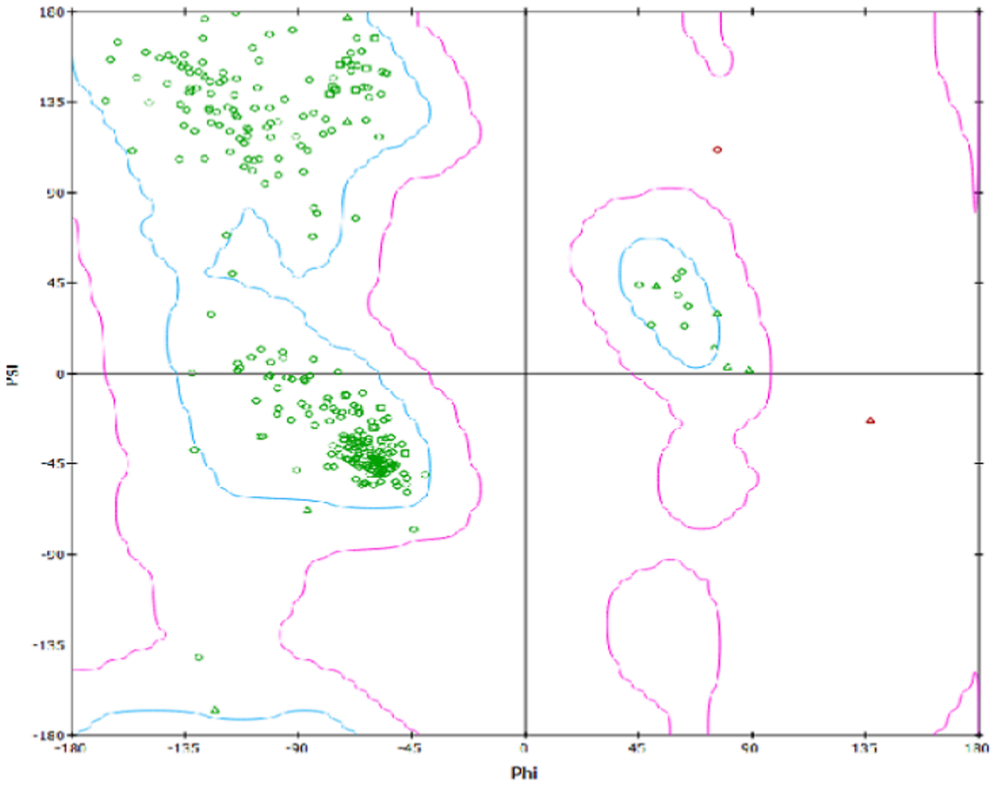

Fig. 11. Ramachandran plot of 4ZRT.

3. Conclusion

Theoretical investigations of the 2B1HID molecule were determined using quantum chemical calculations using DFT. The stability of the molecule was determined at N3-C8 to C6-C7 by 65.47 kcal/mol found by NBO research. With respect to BCP, the AIM topological analysis is used to know the type of bond present in the molecule. The non-covalent interactions are studied using DORI analysis. The HOMO and LUMO energy difference reveals the molecule's biochemical function. Nonlinear optical studies demonstrate the 2B1HID compound's usefulness as an NLO material. MEP studies and Fukui analysis were done to determine the 2B1HID molecule's reactive zones. The UV–Vis spectrum is simulated for different solvents and the maximum absorption wavelength is obtained for DMSO. The thermal stability of the compound is determined using Perl script. 2B1HID can be used for renal disease and it is supported by drug-likeness and docking investigations with a lower binding energy of −6.36 kcal/mol.

CRediT authorship contribution statement

M. Lawrence: Validation, Visualization, Writing – original draft, Writing – review & editing. **P. Rajesh:** Validation, Visualization, Resources, Methodology, Project administration, Software. **Ahmad Irfan:** Data curation, Formal analysis, Funding acquisition, Investigation, Software. **S. Muthu:** Supervision, Validation, Visualization, Resources, Conceptualization, Data curation, Formal analysis, Funding acquisition, Investigation.

Declaration of Competing Interest

The authors declare that they have no known competing financial interests or personal relationships that could have appeared to influence the work reported in this paper.

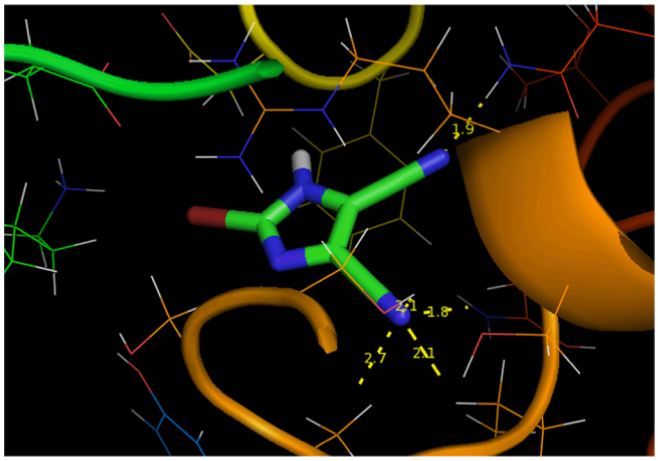

Fig. 12. Docking of 2B1HID with 4ZRT protein.

Data availability

Data will be made available on request.

Acknowledgment

A.Irfan extends his appreciation to the Deanship of Scientific Research at King Khalid University (KKU), Saudi Arabia for funding through large group research project under grant number R.G.P.2/265/44.

References

[1] G. Gautam, B. Parveen, M. Umar Khan, I. Sharma, A. Kumar Sharma, R. Parveen, S. Ahmad, A systematic review on nephron protective AYUSH drugs as constituents of NEERI-KFT (A traditional Indian polyherbal formulation) for the management of chronic kidney disease, Saudi, J. Biol. Sci. 28 (2021) 6441–6453, https://doi.org/10.1016/j.sjbs.2021.07.008.

[2] T.F. Gallegos, C.N. Kamei, M. Rohly, I.A. Drummond, Fibroblast growth factor signaling mediates progenitor cell aggregation and nephron regeneration in the adult zebrafish kidney, Dev. Biol. 454 (2019) 44–51, https://doi.org/10.1016/j.ydbio.2019.06.011.

[3] Y. Saito, S. Yamanaka, N. Matsumoto, T. Takamura, T. Fujimoto, K. Matsui, S. Tajiri, K. Matsumoto, E. Kobayashi, T. Yokoo, Generation of functional chimeric kidney containing exogenous progenitor-derived stroma and nephron via a conditional empty niche, Cell Rep. 39 (2022), 110933, https://doi.org/10.1016/j.celrep.2022.110933.

[4] T. Machiguchi, T. Nakamura, Regenerated nephrons in kidney cortices ameliorate exacerbated serum creatinine levels in rats with adriamycin nephropathy, Biochem. Biophys. Res. Commun. 530 (2020) 541–546, https://doi.org/10.1016/j.bbrc.2020.07.056.

[5] K.M. Morshed, K.E. McMartin, In vitro characterization of renal reabsorption and secretion of folate using primary cultures of human kidney cells, J. Nutr. Biochem. 7 (1996) 276–281, https://doi.org/10.1016/0955-2863(96)00028-9.

[6] L.E. Thompson, M.S. Joy, Endogenous markers of kidney function and renal drug clearance processes of filtration, secretion, and reabsorption, Curr. Opin. Toxicol. 31 (2022), 100344, https://doi.org/10.1016/j.cotox.2022.03.005.

[7] Y. Yang, Y. Li, R. Chen, J. Zheng, Y. Cai, G. Fortino, Risk Prediction of Renal Failure for Chronic Disease Population Based on Electronic Health Record Big Data, Big Data Res. 25 (2021), 100234, https://doi.org/10.1016/j.bdr.2021.100234.

[8] A. Kbirou, H. Hagguir, A. Moataz, M. Dakir, A. Debbagh, R. Aboutaieb, Acute renal failure and bladder tumors, about 106 cases, Nephrol. Ther. 18 (2022) 202–206, https://doi.org/10.1016/j.nephro.2021.10.005.

[9] Y.D. Molla, G.M. Getahun, M.A. Assefa, Giant bladder stone a rare cause of renal failure, a case report, Int. J. Surg. Case Rep. 105 (2023), 108085, https://doi.org/10.1016/j.ijscr.2023.108085.

[10] M.J. Frisch, G.W. Trucks, H.B. Schlegel, G.E. Scuseria, M.A. Robb, J.R. Cheeseman, G. Scalmani, V. Barone, B. Mennucci, G.A. Petersson, H. Nakatsuji, M. Caricato, X. Li, H.P. Hratchian, A.F. Izmaylov, J. Bloino, G. Zheng, J.L. Sonnenberg, M. Hada, D. J. Fox, Gaussian Inc Wallingford, CT, 2009.

[11] R.I. Dennington, T. Keith, J. Millam, GaussView, Version 6, Semichem. Inc, Shawnee Mission, KS, 2016.

[12] G.M. Morris, R. Huey, A.J. Olson, in: Using AutoDock for Ligand-Receptor Docking, Curr Protoc Bioinformatics, John Wiley & Sons Inc, 2008, https://doi.org/10.1002/0471250953.bi0814s24.

[13] S. Yuan, H.C.S. Chan, Z. Hu, Using Pymol as a platform for computational drug design, WIREs Comput. Mol. Sci. 7 (2017) e1298.

[14] T. Lu, F. Chen, Multiwfn: A multifunctional wavefunction analyzer, J Compu. Chem. 33 (2012) 580–592, https://doi.org/10.1002/jcc.22885.

[15] W. Humphrey, A. Dalke, K. Schulten, VMD: Visual molecular dynamics, J. Mol. Graph. 14 (1996) 33–38, https://doi.org/10.1016/0263-7855(96)00018-5.

[16] G.K. Windler, B.L. Scott, N.C. Tomson, P.W. Leonard, Crystal structure of 2-azido-1*H* -imidazole-4,5-dicarbonitrile, Acta Crystallogr E Crystallogr Commun. 71 (2015) o633–o, https://doi.org/10.1107/S2056989015013444.

[17] B.T.G. Lutz, J. Jacob, J.H. van der Maas, Vibrational spectroscopic characteristics of C-H ··· O and N-H ··· π interaction in crystalline N-(2,6-dimethylphenyl)-5-methylisoxazole-3-carboxamide, Vib. Spectrosc 12 (1996) 197–206, https://doi.org/10.1016/0924-2031(96)00018-5.

[18] B. Morzyk-Ociepa, K. Dysz, I. Turowska-Tyrk, D. Michalska, Reinvestigation of the crystal structure, vibrational spectroscopic studies and DFT calculations of 5-bromo-7-azaindole with dual N-H···N hydrogen bonds in dimers, J. Mol. Struct. 1101 (2015) 91–100, https://doi.org/10.1016/j.molstruc.2015.08.003.

[19] A.M. Kini, J.D. Dudek, K.D. Carlson, U. Geiser, R.A. Klemm, J.M. Williams, K. R. Lykke, J.A. Schlueter, H.H. Wang, P. Wurz, J.R. Ferraro, G.A. Yaconi, P. Stout, Do the intramolecular C-C stretching vibrational modes in ET mediate electron-pairing in κ-(ET)2X superconductors? Phys. C Supercond. 204 (1993) 399–405, https://doi.org/10.1016/0921-4534(93)91026-R.

[20] E. Bravanjalin Subi, D. Arul Dhas, S. Balachandran, I. Hubert Joe, Crystal Growth, Structural, Vibrational, Effects of Hydrogen Bonding(C-H…O and C-H…N), Chemical Reactivity, Antimicrobial Activity, Inhibitory Effects and Molecular Dynamic Simulation of 4-Methoxy-N-(Nitrobenzylidene)-Aniline, Polycycl. Aromat. Compd. 43 (2023) 2690–2744, https://doi.org/10.1080/10406638.2022.2052116.

[21] P. Migchels, N. Leroux, Th. Zeegers-Huyskens, Fourier transform infrared spectrometric study of the interaction between hexa-2,4-dienylideneisopropylamine and 3-phenylprop-2-enylideneisopropylamine with model proton donors Part I. Thermodynamic parameters, C-N and OH stretching vibrations, Vib. Spectrosc 2 (1991) 81–88, https://doi.org/10.1016/0924-2031(91)85013-D.

[22] O. Noureddine, N. Issaoui, S. Gatfaoui, O. Al-Dossary, H. Marouani, Quantum chemical calculations, spectroscopic properties and molecular docking studies of a novel piperazine derivative, J. King Saud Univ.-Sci. 33 (2021), 101283, https://doi.org/10.1016/j.jksus.2020.101283.

[23] Jumabaev, U. Holikulov, H. Hushvaktov, N. Issaoui, A. Absanov, Intermolecular interactions in ethanol solution of OABA: Raman, FTIR, DFT, M062X, MEP, NBO, FMO, AIM, NCI, RDG analysis, J. Mol. Liq. 377 (2023) 121552. https://doi.org/10.1016/j.molliq.2023.121552.

[24] J.D.D. Tarika, X.D.D. Dexlin, A.A. kumar, D.D. Jayanthi, A. Rathika, T.J. Beaula, Insights into Weak and Covalent Interactions, Reactivity sites and Pharmacokinetic Studies of 4-Dimethylaminopyridinium Salicylate Monohydrate using Quantum Chemical Computation method, Comput Theor Chem. 1206 (2021) 113483. https://doi.org/10.1016/j.comptc.2021.113483.

[25] S. Mebs, Complex modes of bonding: NCI/ELI-D vs. DORI surface analyses of hapticities and hydrogen–hydrogen contacts in zincocene related compounds, Chem. Phys. Lett. 651 (2016) 172–177, https://doi.org/10.1016/j.cplett.2016.03.046.

[26] J.N.C. Mishma, V.B. Jothy, A. Irfan, B. Narayana, S.N. Kodlady, S. Muthu, Solvent potential effects (topological aspects, electron excitation), spectral characterization and biological attributes of NLO active 1-(2,4-dinitrophenyl)-2-((E)-3-phenylallylidene) hydrazine: Multiple anti tuberculosis agent, J. Mol. Liq. 376 (2023), 121439, https://doi.org/10.1016/j.molliq.2023.121439.

[27] M. Vennila, R. Rathikha, S. Muthu, A. Senthil, A. Jeelani, A. Irfan, Structural vibrational analysis (FT-IR, FT-Raman), electronic studies based on solvents (UV–Vis, non-linear optics, frontier molecular orbitals, molecular electrostatic potential, natural bond orbital and Fukui evaluation) and Hirshfeld surface analysis on 4-chloroacetophenone, J. Indian Chem. Soc. 100 (2023), 100871, https://doi.org/10.1016/j.jics.2022.100871.

[28] V.S. Jeba Reeda, V. Bena Jothy, M. Asif, M. Nasibullah, N.S. Alharbi, G. Abbas, S. Muthu, Synthesis, solvent polarity(polar and nonpolar), structural and electronic properties with diverse solvents and biological studies of (E)-3-((3-chloro-4-fluorophenyl) imino) indolin-2-one, J. Mol. Liq. 380 (2023), 121709, https://doi.org/10.1016/j.molliq.2023.121709.

[29] N. Kateris, A.S. Jayaraman, H. Wang, HOMO-LUMO gaps of large polycyclic aromatic hydrocarbons and their implication on the quantum confinement behavior of flame-formed carbon nanoparticles, Proc. Combust. Inst. (2022), https://doi.org/10.1016/j.proci.2022.07.168.

[30] Prakashgouda G Patil, Raveendra Melavanki, Shivaraj B Radder, Raviraj Kusanur, Chidanandayya S Hiremath, Ninganagouda R Patil, Sudhir M Hiremath, Synthesis, Structural Characterizations, and Quantum Chemical Investigations on 1-(3-Methoxy-phenyl)-3-naphthalen-1-yl-propenone, ACS Omega 6 (2021) 25982-25995. https://doi.org/10.1021/acsomega.1c02688.

[31] K. Satheeshkumar, P. Saravana Kumar, R. Shanmugapriya, C. Nandhini, K. N. Vennila, K.P. Elango, Ratiometric fluorescence sensing of hypochlorite ion by dansyl hydrazine - Spectroscopic and TD-DFT studies, J. Mol. Struct. 1275 (2023), 134719, https://doi.org/10.1016/j.molstruc.2022.134719.

[32] N. Al-Maharik, M. Daqqa, A. AlObaid, A. Zarrouk, I. Warad, Synthesis, crystal structure, physicochemical of new (±)-2,7-dimethoxy-3-(4-metho-xyphenyl)-3-methylchroman-4-one: DFT, Hirshfeld, optical and TD-DFT/DFT analysis, J. Mol. Struct. 1286 (2023), 135536, https://doi.org/10.1016/j.molstruc.2023.135536.

[33] R. Kobayashi, R.D. Amos, The application of CAM-B3LYP to the charge-transfer band problem of the zincbacteriochlorin–bacteriochlorin complex, Chem. Phys. Lett. 420 (2006) 106–109, https://doi.org/10.1016/j.cplett.2005.12.040.

[34] B. Komjáti, Á. Urai, S. Hosztafi, J. Kökösi, B. Kováts, J. Nagy, P. Horváth, Systematic study on the TD-DFT calculated electronic circular dichroism spectra of chiral aromatic nitro compounds: A comparison of B3LYP and CAM-B3LYP, Spectrochim. Acta A Mol. Biomol. Spectrosc. 155 (2016) 95–102, https://doi.org/10.1016/j.saa.2015.11.002.

[35] M. Vennila, R. Rathikha, S. Muthu, A. Jeelani, A. Irfan, Theoretical structural analysis (FT-IR, FT-R), solvent effect on electronic parameters NLO, FMO, NBO, MEP, UV (IEFPCM model), Fukui function evaluation with pharmacological analysis on methyl nicotinate, Comput Theor Chem. 1217 (2022), 113890, https://doi.org/10.1016/j.comptc.2022.113890.

[36] M.S. Mohamed Ahmed, A.E.M. Mekky, S.M.H. Sanad, Regioselective [3 + 2] cycloaddition synthesis and theoretical calculations of new chromene-pyrazole hybrids: A DFT-based Parr Function, Fukui Function, local reactivity indexes, and MEP analysis, J. Mol. Struct. 1267 (2022), 133583, https://doi.org/10.1016/j.molstruc.2022.133583.

[37] M.L. Beatrice, S.M. Delphine, M. Amalanathan, M.S.M. Mary, H.M. Robert, K. T. Mol, Molecular structure, spectroscopic, Fukui function, RDG, anti-microbial and molecular docking analysis of higher concentration star anise content compound methyl 4-methoxybenzoate-DFT study, J. Mol. Struct. 1238 (2021), 130381, https://doi.org/10.1016/j.molstruc.2021.130381.

[38] P.P. Zamora, K. Bieger, A. Cuchillo, A. Tello, J.P. Muena, Theoretical determination of a reaction intermediate: Fukui function analysis, dual reactivity descriptor and activation energy, J. Mol. Struct. 1227 (2021), 129369, https://doi.org/10.1016/j.molstruc.2020.129369.

[39] V.S. Jeba Reeda, V. Bena Jothy, Vibrational spectroscopic, quantum computational (DFT), reactivity (ELF, LOL and Fukui), molecular docking studies and molecular dynamic simulation on (6-methoxy-2-oxo-2H-chromen-4-yl) methyl morpholine-4-carbodithioate, J. Mol. Liq. 371 (2023), 121147, https://doi.org/10.1016/j.molliq.2022.121147.

[40] S. Selvakumari, K. Murthy Potla, D. Shanthi, A. Irfan, S. Muthu, Solvent effect on molecular, electronic parameters, topological analysis and Fukui function evaluation with biological studies of imidazo [1, 2-a] pyridine-8-carboxylic acid, J Mol Liq. 382 (2023) 121863. https://doi.org/10.1016/j.molliq.2023.121863.

[41] S.K. Alghamdi, F. Abbas, R.K. Hussein, A.G. Alhamzani, N.T. El-Shamy, Spectroscopic characterization (IR, UV-Vis), and HOMO-LUMO, MEP, NLO, NBO Analysis and the Antifungal Activity for 4-Bromo-N-(2-nitrophenyl) benzamide; Using DFT Modeling and In silico Molecular Docking, J Mol Struct. 1271 (2023), 134001, https://doi.org/10.1016/j.molstruc.2022.134001.

[42] N. Boukabcha, A. Benmohammed, M.H.M. Belhachemi, M. Goudjil, S. Yahiaoui, Y. Megrouss, A. Djafri, N. Khelloul, Z.D. Benyehlou, A. Djafri, A. Chouaih, Spectral investigation, TD-DFT study, Hirshfeld surface analysis, NCI-RDG, HOMO-LUMO, chemical reactivity and NLO properties of 1-(4-fluorobenzyl)-5-bromolindolin-2,3–dione, J. Mol. Struct. 1285 (2023), 135492, https://doi.org/10.1016/j.molstruc.2023.135492.

[43] M. Sumithra, N. Sundaraganesan, K. Venkata Prasad, R. Rajesh, V. Vetrivelan, V. Ilangovan, A. Irfan, S. Muthu, Effect of green solvents physical, chemical, biological and bonding nature on 5-acetyl-thiophene-2-carboxylic acid by DFT and TD-DFT approach – An antiviral agent, J. Indian Chem. Soc. 100 (2023), 100867, https://doi.org/10.1016/j.jics.2022.100867.

[44] S. Lakra, S. Kumar Mukherjee, Study of structural, electronic, optical and thermodynamic properties of SnSiO3 compound: A DFT study, Mater. Today:. Proc. (2023), https://doi.org/10.1016/j.matpr.2023.01.231.

[45] I. Jomaa, N. Issaoui, T. Roisnel, H. Marouani, Insight into non-covalent interactions in a tetrachlorocadmate salt with promising NLO properties: Experimental and computational analysis, J. Mol. Struct. 1242 (2021), 130730, https://doi.org/10.1016/j.molstruc.2021.130730.

[46] AL-Adhreai, M. ALSaeedy, A. Alrabie, I. Al-Qadsy, S. Dawbaa, Z.M. Alaizeri, H.A. Alhadlaq, A. Al-Kubati, M. Ahamed, M. Farooqui, Design and synthesis of novel enantiopure Bis(5-Isoxazolidine) derivatives: insights into their antioxidant and antimicrobial potential via in silico drug-likeness, pharmacokinetic, medicinal chemistry properties, and molecular docking studies, Heliyon. 8 (2022) e09746. https://doi.org/10.1016/j.heliyon.2022.e09746.

[47] S. Gatfaoui, A. Mezni, T. Roisnel, H. Marouani, Synthesis, characterization, Hirshfeld surface analysis and antioxidant activity of a novel organic-inorganic hybrid material 1-methylpiperazine-1,4-diium bis(nitrate), J. Mol. Struct. 1139 (2017) 52–59, https://doi.org/10.1016/j.molstruc.2017.03.028.

[48] H. Ahmad, G. Khan, Serdaroğlu, Physicochemical properties, drug likeness, ADMET, DFT studies, and in vitro antioxidant activity of oxindole derivatives, Comput. Biol. Chem. 104 (2023), 107861, https://doi.org/10.1016/j.compbiolchem.2023.107861.

[49] H. Tomar, A. Rawat, K. Nagarkoti, O. Prakash, R. Kumar, R.M. Srivastava, S. Rawat, D.S. Rawat, Ocimum gratissimum L. and Ocimum sanctum L.: Comparative compositional analysis of essential oils and in-vitro biological activities with in-silico PASS prediction and ADME/Tox studies, S. Afr. J. Bot. 157 (2023) 360–371, https://doi.org/10.1016/j.sajb.2023.04.014.

[50] F. Carrascoza, S. Zaric, R. Silaghi-Dumitrescu, Computational study of protein secondary structure elements: Ramachandran plots revisited, J. Mol. Graph. Model. 50 (2014) 125–133, https://doi.org/10.1016/j.jmgm.2014.04.001.

[51] S.N. Sahu, S.S. Satpathy, S. Pattnaik, C. Mohanty, S.K. Pattanayak, Boerhavia diffusa plant extract can be new potent therapeutics against mutant nephrin protein responsible for type1 nephrotic syndrome: Insight into hydrate-ligand docking interactions and molecular dynamics simulation study, J. Indian Chem. Soc. 99 (2022), 100669, https://doi.org/10.1016/j.jics.2022.100669.

[52] M. Malar Wezhli, P. Balamurugan, K. Raju, S. Sevvanthi, A. Irfan, S. Javed, S. Muthu, Quantum computational, spectroscopic, topological investigations and molecular docking studies on piperazine derivatives: A comparative study on Ethyl, Benzene and Furan sulfonyl Piperazine, J. Mol. Struct. 1274 (2023), 134324, https://doi.org/10.1016/j.molstruc.2022.134324.

[53] S.B. Radder, R. Melavanki, U. Radder, S.M. Hiremath, R. Kusanur, S. S. Khemalapure, Synthesis, spectroscopic (FT-IR, FT-Raman, NMR), reactivity (ELF, LOL and Fukui) and docking studies on 3-(2–hydroxy-3–methoxy-phenyl)-1-(3-nitro-phenyl)-propenone by experimental and DFT methods, J. Mol. Struct. 1255 (2022), 132443, https://doi.org/10.1016/j.molstruc.2022.132443.

[54] S.B. Radder, R. Melavanki, S.M. Hiremath, R. Kusanur, S.S. Khemalapure, S. Christopher Jeyaseelan, Synthesis, spectroscopic (FT-IR, FT-Raman, NMR & UV-Vis), reactive (ELF, LOL, Fukui), drug likeness and molecular docking insights on novel 4-[3-(3-methoxy-phenyl)-3-oxo-propenyl]-benzonitrile by experimental and computational methods, Heliyon 7 (2021) e08429.

[55] Sudhir M. Hiremath, Vibrational, electronic and reactivity insight on (5-chloro-benzofuran-3-yl)-acetic acid hydrazide: A Spectroscopic and DFT approach, J. Mol. Struct. https://doi.org/10.1016/j.molstruc.2021.130479.